Structural Engineering and Mechanics, Vol. 5, No. 4 (1997) 451-469
DOI: http://dx.doi.org/10.12989/sem.1997.5.4.451

Behaviour of laminated elastomeric bearings

A. Mori†

Japan Engineering Consultants, Tokyo, Japan

P. J. Moss‡, A. J. Carr‡† and N. Cooke‡‡

University of Canterbury, Christchurch, New Zealand

Abstract. Experimental work undertaken to investigate the behaviour of laminated elastomeric bridge bearings under compression and a combination of compression and shear or rotation has been reported on elsewhere. However, it is difficult to determine the state of stress within the bearings in terms of the applied forces or the interaction between the steel shims and the rubber layers in the bearings. In order to supply some of the missing information about the stress-strain state within the bearings, an analytical study using the finite element method was carried out. The available experimental results were used to validate the model after which the analyses were used to provide further information about the state of stress within the bearing.

Key words: bridge bearings; elastomeric rubber bearings; finite element analysis; compression; shear strain; rotation.

1. Introduction

Experimental work to investigate the behaviour of laminated elastomeric bridge bearings under compression, and a combination of compression and shear or rotation has been reported previously (Mori 1993, Mori, *et al.* 1996). However, this experimental work did not provide any information on the interaction between the steel shims and rubber layers in the bearings which is important when considering the critical states of stress in the bearings.

A key factor in the design of laminated elastomeric bearings is the level of shear strain in the elastomer of the bearings under the design load combinations. The methods used to calculate this are based on assumptions about the deformation capability of the bearings. However, it is difficult to determine the strain state of the bearings in terms of the applied forces on account of a lack of knowledge of the stress-strain state inside the bearings.

In order to supply some of the missing information about the stress-strain state within a bearing, an analytical study was carried out by modelling a bearing using the Finite Element Method (FEM). The analytical results are compared with the experimental results in order to

† Engineer, Earthquake Disaster Mitigation Department
‡ Associate Professor, Department of Civil Engineering
‡† Reader, Department of Civil Engineering
‡‡ Senior Lecturer and Head, Department of Civil Engineering

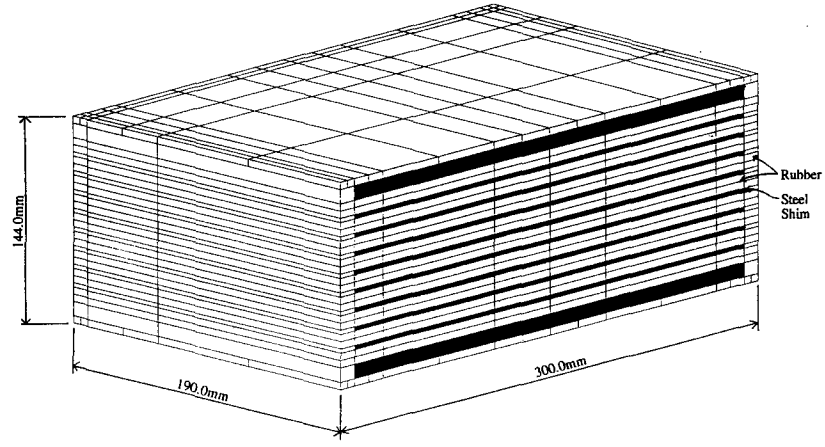

Fig. 1 Analysis model for an elastomeric bearing (one half model for analyses in shear).

verify the analytical model. From the analytical model it was possible to: investigate the stress-strain level in the bearing and the interaction between the rubber and steel shims; verify the reliability of the existing methods for estimating the strain level in the elastomer; and attempt to determine the ultimate state in the bearing.

2. Verification of the numerical model

Several models, varying in terms of the degree of mesh discretization, were evaluated (Mori 1993). The model chosen for the main analyses is illustrated in Fig. 1. The elements used to model both the rubber and the steel shims were 20-node isoparametric brick elements. The construction of the bearing modelled comprised nine 10 mm thick rubber layers interspersed with eight 3 mm thick steel shim reinforcements. The outer steel plates were 10 mm thick with 5 mm thick top and bottom cover rubber layers. The side rubber cover was 10 mm thick. Of the total bearing height of 144 mm, the total rubber thickness was 100 mm.

Since rubber exhibits nonlinear elastic behaviour under elongation, compression and shear, and has a large deformation capability, it was necessary to determine its constitutive behaviour for use in the modelling. The theoretical study of rubber elasticity began in the 1930's (Treloar 1958) and several forms of the strain energy function of rubber-like materials have been proposed (Atkin and Fox 1980) as the basis for determining the constitutive relationship for rubber. In the present numerical study, the Mooney-Rivlin form of the strain energy function was used. The constitutive equation involves coefficients that depend on rubber properties such as the modulus of elasticity, shear modulus, or degree of rubber hardness, which can be obtained from simple material tests. In this case, standard tensile tests were carried out to obtain the tensile stress-strain response illustrated in Fig. 2.

The ABAQUS (1992) computer program used to carry out the analyses could model both the polynomial and Ogden forms of the strain energy potential, the Mooney-Rivlin form being a particular case that could be obtained from either form. In the analyses, first or second order curves were directly fitted to the tensile stress-strain test results to obtain the necessary parameters for the Mooney-Rivlin form of the strain energy potential. It was found that the first order

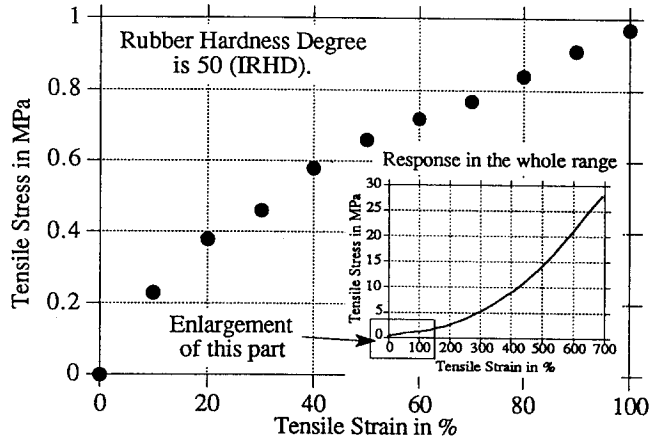

Fig. 2 Tensile stress-strain response of rubber test specimens.

curve fitted the tensile test data very well up to a strain of about 100%, while the second order curve fitted the tensile test data well up to a strain of 250~300%.

However, the analyses indicated that a modification was required to the stress-strain relationships for the rubber as determined from standard small test specimens and shown in Fig. 2. After several analyses using different modification factors, it was found that a factor of 0.7 times the original stress-strain relationship gave a reasonable agreement with the experimental data as can be seen in the results presented in the sections that follow.

2.1. Compression

2.1.1. Force-displacement response

The analytical results for the compressive force-displacement response are compared with the experimental results in Fig. 3.

2.1.2. Normal-stress distributions

Fig. 4 compares the experimental (Mori, *et al.* 1996) and analytical normal stress ratios, σ/σ_0, where σ is the normal stress and σ_0 is the average compressive stress on the bearing along both centrelines. It can be seen that the analytical and experimental results show good agreement, with the average compressive stresses, σ_0, differing some 4% between the analytical and experimental values.

2.2. Shear

2.2.1. Force-displacement response

The analytical model for shear comprised one half of the bearing using symmetry to minimise computational effort. The stops that were used in the tests to prevent the bearings from slipping

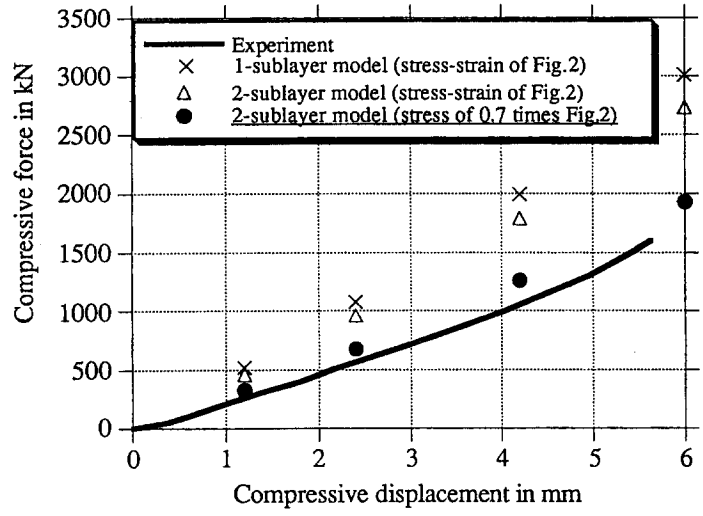

Fig. 3 Comparison of the experiment and analysis of the vertical force-displacement response.

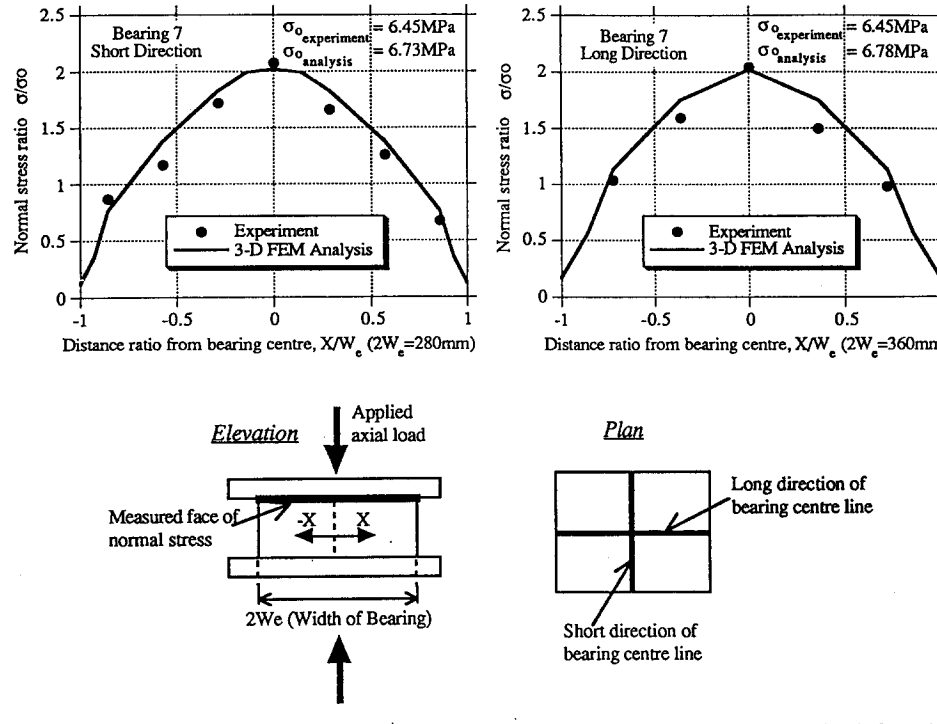

Fig. 4 Comparison of the normal stress distribution of the experiment and analysis, left - short direction -, right - long direction -.

were modelled by setting the horizontal degree of freedom for the edge nodes of the outer steel plates and the rigid surface elements to move together.

Since the analysis was controlled by prescribed displacements rather than by applied forces, it was necessary to choose analytical results that had similar compressive forces to the experimen-

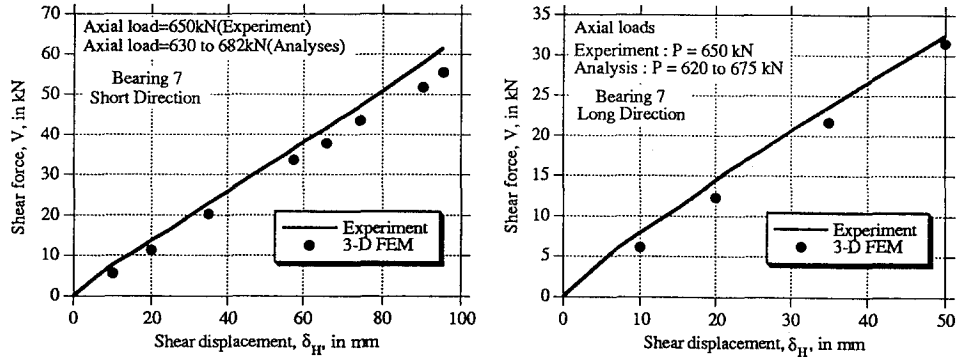

Fig. 5 Comparison of the experiment and analysis in terms of the shear force - displacement response, left - short direction -, right - long direction -.

tal applied axial loads for the various analysis cases. When a prescribed constant compressive displacement is used in the analysis as the shear displacement is increased, the equivalent compressive force decreases because of the hardening of the bearing behaviour in shear.

Fig. 5 compares the experimental and analytical force-displacement responses for shearing in the long and short directions of the bearings. While there are some differences between the experimental and analytical results, the shear stiffnesses (given by the slope of the force/displacement relationship) are similar.

2.2.2. Normal stress distributions

The normal stress distributions along the centreline of the top face of the bearing under shear are compared in Fig. 6. It can be seen that there is a change in the shape of the normal stress distribution as the bearing shear strain increases from 22% to 106%. While there are some differences between the experimental and analytical results, the general trends in the distributions are similar. The largest difference between the experimental and analytical results occurs at the second point from the left hand end in the figure, and this is probably caused by an experimental error in the small load cell used to measure the normal force at this point on the bearing (Mori, *et al.* 1996).

2.3. Rotation

2.3.1. Moment-rotation response

In the analytical bearing model, rigid surface elements were used to provide rigid boundary surfaces to bear on the bearing. In the analyses, a moment was generated by setting the rigid boundary to incline while keeping the vertical displacement at the centre constant as this was equivalent to keeping the normal force constant. The comparison of experimental and analytical moment-rotation results in the short direction of the bearing is given in Fig. 7. The rotational stiffnesses (given by the slopes) are similar and show the same trend as seen in the force-displacement responses in compression and shear.

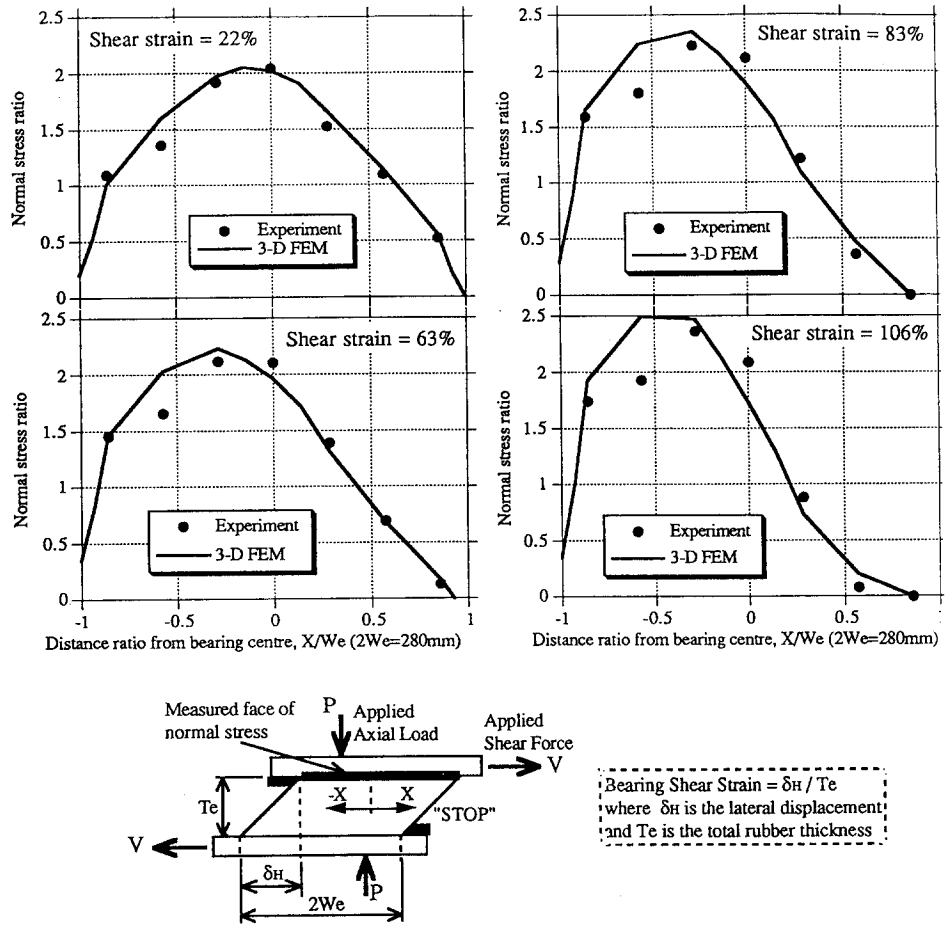

Fig. 6 Comparison of the experiment and analysis in terms of the normal stress distributions as the bearing shear strain increases under a design axial load of 650 kN (the short direction of Bearing 7).

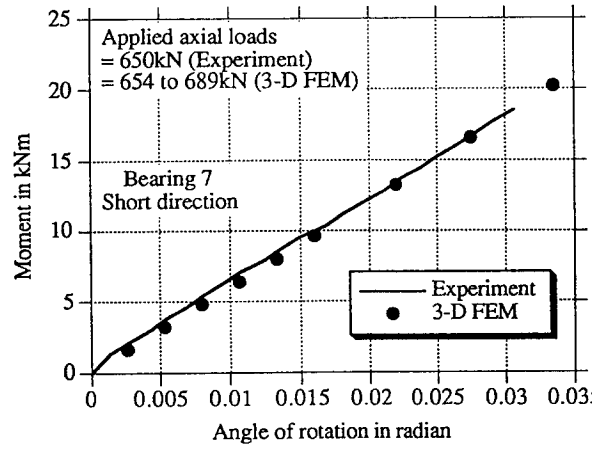

Fig. 7 Comparison of the experiment and analysis in terms of the moment-rotation response in the short test direction.

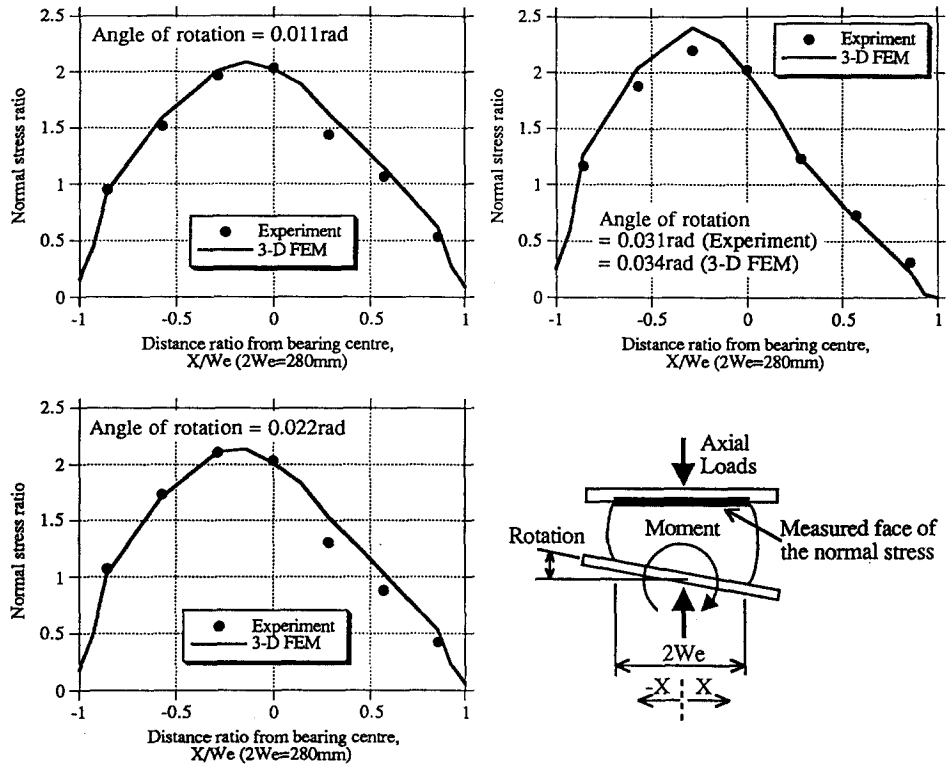

Fig. 8 Comparison of the experiment and analysis in terms of the normal stress distributions as angle of rotation increases (short direction of Bearing 7 under the design axial load of 650 kN).

2.3.2. Normal stress distribution

The comparisons of the normal stress distributions on the centreline of the top face of the bearing are shown in Fig. 8 for various angles of rotation. It can be seen that the analytical results are in close agreement with the experimental values.

3. Further numerical investigations

3.1. Normal stress distributions

Since the finite element model was three dimensional, it is possible to investigate the normal stress distribution over the whole bearing face under a combination of compressive and shear loads. This is illustrated by Fig. 9 for the cases of 0, 64 and 106% shear strain. The plan area of the normal stress distribution can be seen to decrease as the shear deformation increases and the maximum stress intensity increases with the increasing shear deformation.

The stress distribution on the bearing face is affected by the coefficient of friction between the bearing face and the external surfaces. For the analyses reported herein, a coefficient of friction of 0.25 was found to be a suitable value (Mori 1993). With this value for the coefficient

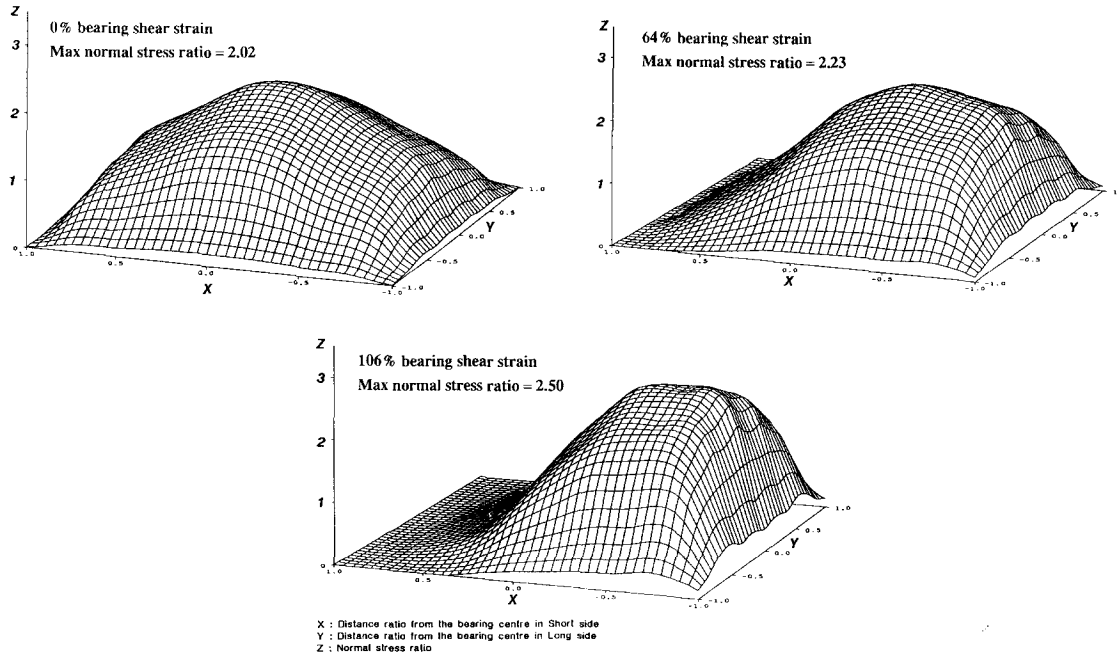

Fig. 9 Normal stress distributions on the bearing top face under shear and compression.

of friction, the normal stress around the edge was almost zero whereas if the interface should have a higher friction co-efficient, the normal stress at all the edges would be higher because of the higher friction forces.

3.2. Deformation under compression

Under compression, only the rubber in the bearing deforms. The lateral deformation of the rubber layer generates lateral stresses such as shear and lateral tensile stresses leading to a budging deformation at the edges of each rubber layer to satisfy force equilibrium in each layer.

Fig. 10 shows the deformation at the central cross-section of the bearing under the design compression load.

It can be seen that each layer is evenly compressed. Large shear strains occur at the edges on account of the bulging deformation, and this is an important factor in the design of elastomeric bearings. This is discussed further in a later section.

The lateral tensile and shear strains developed between an inner rubber layer and a steel shim near the edge (the interface between the inner rubber and the cover layer) are shown in Fig. 11 as a function of the bearing compressive strain (defined as the vertical displacement of the bearing divided by the total rubber thickness in the bearing). Under relatively small strains, the lateral tensile and shear strains are similar but as the compressive strain increases, the difference between them becomes significant as the lateral tensile strain grows rapidly while the shear strain changes more slowly.

Fig. 12 shows the lateral bulging deformations at the bearing edge of a rubber layer just inside the cover rubber. Because of the large bulging deformation, the edge angle of the bulge

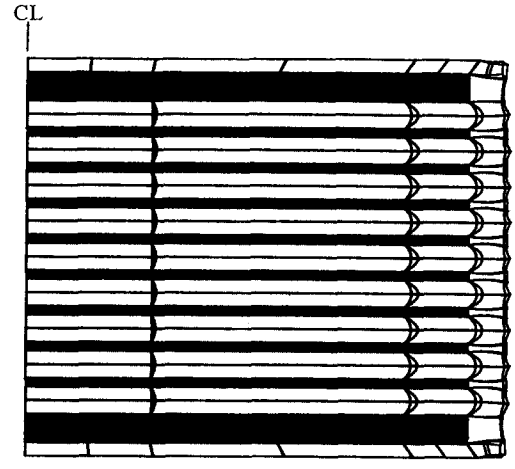

Fig. 10 Bearing deformation under compression (design load level).

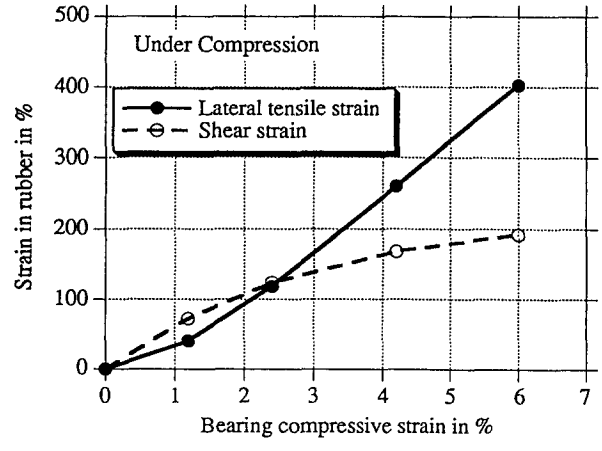

Fig. 11 Maximum lateral tensile and shear strains obtained between a rubber layer and a steel shim versus bearing compressive strains.

reaches 75° from the vertical at a compressive strain of 6%. At this stage, the lateral tensile strain component is greater than the shear strain. The shear strain is the more dominant strain until the bearing compressive strain reaches 2.4% at which strain the edge angle of the bulge makes an angle of 45 from the vertical.

3.3. Deformation under shear

The deformation at the central cross-section of a bearing under a bearing shear strain of 106% is shown in Fig. 13. The elements representing the edge cover rubber show a complicated distortion and this was found to introduce a numerical difficulty in forming the element stiffness, thus limiting the shear strain that could be reached using this mesh. A finer mesh could be used to represent the edge cover rubber but only at the cost of increasing the computational effort required.

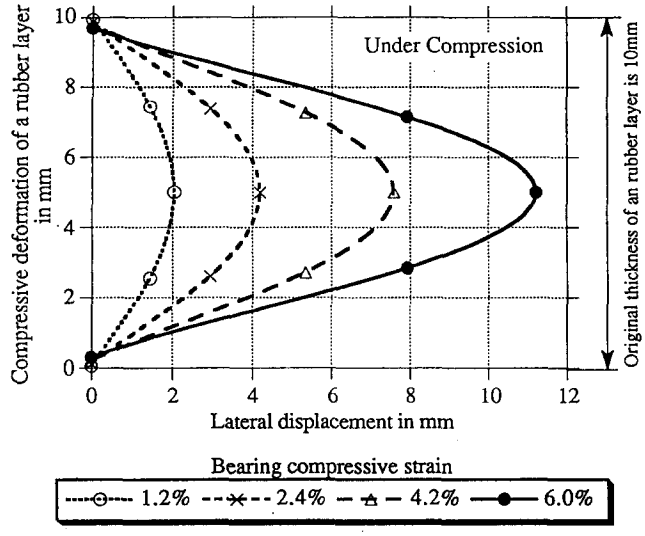

Fig. 12 Lateral bulging deformation of a rubber layer under various bearing compressive strains.

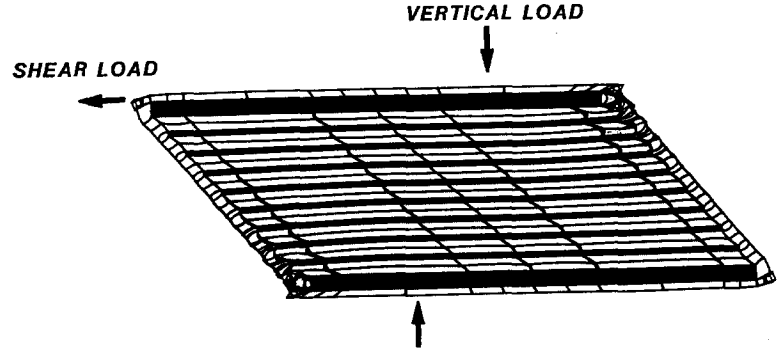

Fig. 13 Bearing deformation under a bearing shear strain of 106%.

It can also be seen that the steel shims in the bearing undergo marked bending at the edges. The definition of the yield surface for isotropic elasto-plastic materials used in the commercial finite element package used (ABAQUS 1992) follows the von Mises yield criterion which defines the material yield as occurring when the square root of the difference between the principal stresses in the three-dimensional state reaches the yield stress value as measured in a standard tension test. The yield state is thus described by:

$$(\sigma_1-\sigma_2)^2+(\sigma_2-\sigma_3)^2+(\sigma_3-\sigma_1)^2=2\sigma_{sy}^2 \tag{1}$$

where $\sigma_i (i=1, 2, 3)$ are the principal stresses and σ_{sy} is the yield stress in uni-axial tension. The yield surface defined by Eq. (1) is ellipsoidal.

From the analytical results, the maximum von Mises stress of 239 MPa generated in the steel shims near the edges at the top and bottom of the bearing nearly reached the uni-axial steel yield stress of 250 MPa at a bearing shear strain of 106%. In the shear tests carried out (Mori 1993, Mori, *et al*, in press 1997b) up to 150% bearing shear strain for bearing No. 2,

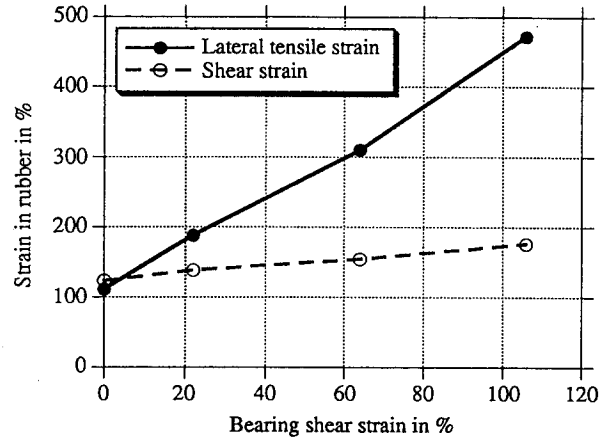

Fig. 14 Maximum lateral tensile and shear strains obtained between the first inner rubber layer and the outer steel plate versus bearing shear strains.

it was found subsequently that the 3 mm steel shims had become bent from the large flexural stresses caused by the rubber lateral bulging deformation. No yielding of the steel shims caused by the hysteretic behaviour could be detected after the tests even though the shear stiffness of the bearing changed at different stages of loading and unloading. While this stiffness change is most likely due to the rubber strain crystallisation effect at large strains, it is possible that yield of the steel shims occurs at bearing shear strains of between 106% and 150% under an applied axial load of 650 kN, for bearings having the dimensions shown in Fig. 1.

The lateral tensile and shear strains that occurred between the first inner rubber layer and the outer steel plate near the edge of the interface between the inner rubber and the cover rubber is shown in Fig. 14. The behaviour of the lateral tensile and shear strains under shear and compression is similar to that under compression only (compare Fig. 11). The bearing shear strain contributes more to the lateral tensile strain than to the shear strain, because of the similar lateral projecting bulge to that occurring at the edge of the bearing under compression. It was found that the shear strain in the cover rubber was more than 1.5 times larger than the shear strain at the inner rubber at 106% bearing shear strain. This indicates that as the shear strain increases there is the possibility of the rubber rupturing at the edge of the bearing near the interface between the cover and inner layers of rubber since the rupture strain in uni-axial tension was about 700% (Mori 1993).

3.4. Deformation under rotation

Fig. 15 shows the bearing deformation at an angle of rotation of 0.0335 radians. The lateral tension and shear strains that occur between the first inner rubber layer and the outer steel plate are shown in Fig. 16 and show similar trends to the other two loading states. The strains in the rubber under an angle of rotation of 0.0335 radians (1.9°) are approximately equivalent to the strains under a shear strain of some 50% (Fig. 11).

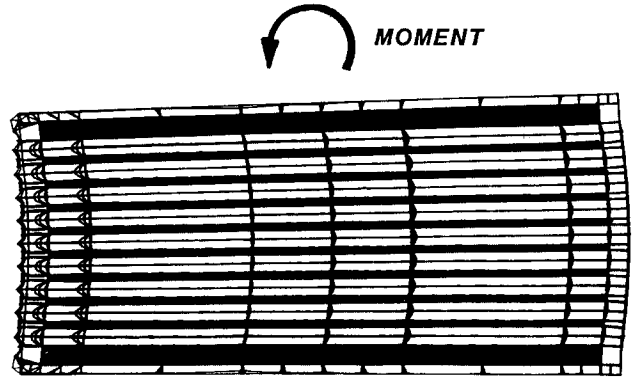

Fig. 15 Bearing deformation under an angle of rotation of 0.0335 radians.

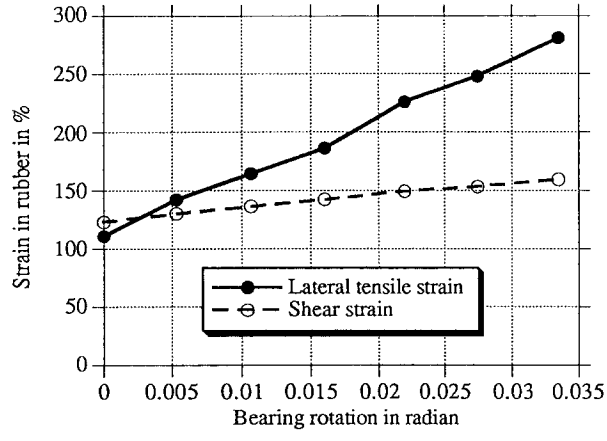

Fig. 16 Maximum lateral tensile and shear strains obtained between the first inner rubber layer and the outer steel plate under the various angles of rotation.

3.5. Bearing behaviour in tension

The rubber in a bearing under goes large shear strains under even small bearing tensile strains which may occur by accident, such as could occur in uplift due to seismic inertia forces in the superstructure of a bridge. An analytical study was carried out in order to investigate the bearing behaviour in tension.

Using symmetry, the model used in the analysis represented one eight of the whole bearing with a fixed boundary condition being applied between the external rigid plate and the outer thick steel plate of the bearing. The analysis was carried out up to the point where the tensile strain reached 5% because, as can be seen in Fig. 17, the distortions at the edge cover rubber appeared to be similar to those shown in Fig. 13 and 15. The bearing deformation under tension is a mirror image of that of compression with a lateral inward bulging deformation of the rubber layers and the normal stress contours in Fig. 17 show a similar stress hill to that under compression, but of opposite sign.

Fig. 18 shows the tensile-displacement response of the bearing and the lateral tensile and

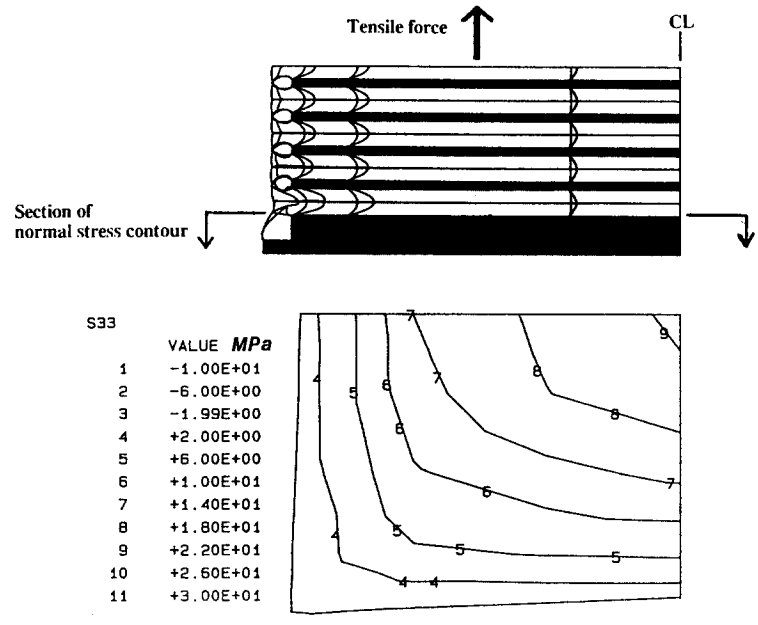

Fig. 17 Bearing deformation (only 1/8 part is shown) and normal stress contour (1/4 part is shown) under a bearing tensile strain of 5%.

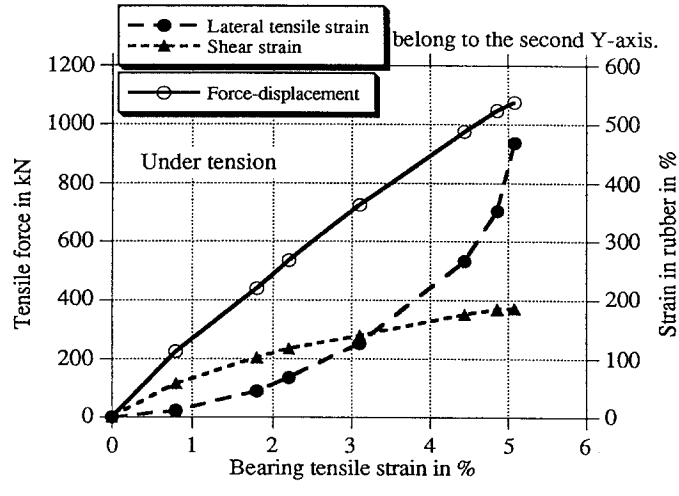

Fig. 18 Bearing performance under tension in terms of force-strain, lateral tensile and shear strains obtained between the first inner rubber layer and the outer steel plate.

shear strains between the first inner layer and the outer steel plate at the edge of the interface between the inner rubber and the cover rubber as a function of the bearing tensile strain. The force-displacement response is slightly non-linear and as was found for the compression analyses, the shear strain tends to an asymptotic value as the bearing tensile strain increases while the lateral tensile strain increases rapidly, and would lead to rupture of the rubber at the edges of the bearing at higher tensile strains.

Table 1 Comparison of the obtained maximum shear strains due to compression

Bearing compression strain	3-D FEM	BE1/76 & AASHTO	Japanese manual	BS5400
1.2%	72%	57%	81%	103%
2.4%	123%	113%	160%	213%
4.2%	168%	199%	282%	398%
6.0%	192%	284%	402%	607%

4. Considerations for design

Previous papers have described how the maximum permissable shear strain in the rubber produced by the different loadings is an important factor in the design of elastomeric bearings. In this section, the shear strains calculated using several available design procedures are compared with those obtained analytically for the same loading conditions in order to investigate the apparent safety margins of the design methods for laminated elastomeric bearings.

The design methods considered are those of BE1/76 (High. Dir 1976), B5400 (BSI 1983), the Japanese Manual for the Design of Base-Isolated Highway Bridges (Min. Constr. 1992), and the AASHTO Guide Specification for Seismic Isolation Design of Highway Bridges (1990). The equations used for calculating the maximum shear strains caused by the different loadings are given in Appendix A. The tensile stress developed in the steel shims of the bearing is calculated using the equation given in the design codes and is compared with the analytically evaluated value.

4.1. Comparison of analytical and design shear strains

4.1.1. Shear strain due to compression

In order to calculate the maximum shear strain due to compression using the design equations it is necessary to calculate the bearing compressive strain, ε_c, as given by Eq. (A2). However, the design equations for compressive stiffness are not very accurate (Mori, *et al.* 1996) and therefore the bearing compressive strain is calculated as a ratio of the total applied vertical displacement to the total rubber thickness of the bearing used in the analyses reported in the previous section instead of using Eq. (A2). In BS5400 the maximum shear strain due to due compression, γ_c, is calculated using Eq. (A2) because the equation does not explicitly use the bearing compressive strain ε_c.

Table 1 summarises the maximum shear strain due to compression under the various bearing compressive strains obtained from the 3-D FEM analysis and Eqs. (A1) and (A3) for the bearing design. A bearing compressive strain of 2.4% is equivalent to the design axial load level and, as discussed earlier (see Fig. 12), the shear strain in the rubber is more dominant than the other strains only in the vicinity of the design axial load level. From the comparisons in the Table, the equation for the shear strain due to compression provided in BE1/76 and AASHTO is in good agreement with the analytical value at the design load but the Japanese manual

Table 2 Comparison of the maximum total shear strains due to combined loadings (FEM and design methods)

Loading State	Compression	Compression & Shear		Compression & Rotation	
Loading Combination amount of loading	compression 2.4%	compression 3.6%	shear 106%	compression 2.4%	rotation 0.0335 rad
3-D FEM	123%	176%		159%	
BE 1/76 and AASHTO	113%	276% (170%+106%)		244% (113%+131%)	
BS5400	213%	416% (310%+106%)		344% (213%+131%)	

and BS5400 tend to overestimate the values. The design equations indicate linearly increasing shear strain as the bearing compressive strain increases while the 3-D FEM analysis shows non-linearity within creasing shear strain. It is assumed in the design equations that the growing bulge at the bearing edges contributes only to the shear strain.

The difference in the maximum shear strain calculated by BE1/76 (and AASHTO) and the Japanese manual is affected by the coefficient for the bearing shape, C_c which is taken as 6.0 for BE1/76 (AASHTO) and 8.5 for the Japanese manual. Eq. (A3) from BS5400 gives twice the shear strain calculated using BE1/76. The derivation of the equation used in BS5400 is not clear.

4.2. Superposition of shear strain due to combinations of different loadings

When combined axial and shear loads or axial and rotation loads are applied to a bearing, most design methods evaluate the maximum total shear strain due to the combination of different loads as the summation of the estimated shear strains produced by each individual load. These loads are such that they produce a bearing compression strain of 2.4%, a bearing shear strain of 106% under a bearing compressive strain of 3.6%, and an angle of bearing rotation of 0.0335 radians under a bearing compressive strain of 2.4%. The maximum shear strains computed by the FEM analyses at the interface between the rubber layer and the steel shim near the bearing edges under the various load combinations are listed in Table 2 along with the total shear strains calculated using the equations for the bearing design given in Eqs. (A1)-(A10) in Appendix A.

It can be seen from Table 2 that all the design methods give a predicted maximum total shear strain that is much higher than those obtained from the FEM analysis. This is not surprising as the design methods were intended to provide a simple and convenient approximation to the true but analytically more complicated state of stress in the bearings under combined loadings.

It is difficult to discuss the significance of the limits on the maximum total shear strain allowed by the design codes since the design limits are empirically based on the relationship between the design equations and the fatigue tests for the elastomeric bearings. The maximum shear strains generated in the rubber due to shear and rotation movements of the bearing as determined by the FEM analysis are much less than the values given by the design methods. This is because the shear strain component in the rubber gradually transfers to a tensile strain component as the shear and rotation increase (as explained in previous sections). BS5400 predicts a very high

maximum total shear strain but allows a maximum design bearing shear strain of 70%. In comparison, the analytically determined bearing shear strain of 106% is well beyond this limit stipulated in BS5400.

4.3. Tensile stress in the reinforcement

The theoretical tensile stress, σ_{st}, in the steel shim reinforcement for infinite strip bearings has been derived by Stanton and Roeder (1982) using Ghent's theory (Ghent and Meinecke, 1970) and is given by

$$\sigma_{st} = 1.5\left(\frac{t_{e1}+t_{e2}}{2t_s}\right)\sigma_0 \tag{2}$$

for reasonable large shape factors, where

σ_0 is the mean compressive stress on the bearings

t_s is the thickness of the steel shim reinforcement, and

t_{e1} and t_{e2} are the thicknesses of the rubber layers on each side of the steel reinforcement

In the case of the bearing considered in the analysis, t_{e1} and t_{e2} are both 10 mm, t_s is 3 mm and σ_0 is 6.73 MPa; thus, $\sigma_{st}=33.5$ MPa. This value is some 13% lower than that obtained from the FEM analysis.

BE1/76 stipulates that the thickness of the steel shim reinforcement in the bearings is given by:

$$t_s \geq \frac{2(t_{e1}+t_{e2})F}{A_{re}\sigma_{st}} \geq 1.5\text{ mm} \tag{3}$$

where t_s, t_{e1} and t_{e2} are as given above, F is the axial load and A_{re} is the reduced effective cross-sectional area as before.

In BS5400, the thickness of the steel shim is given by:

$$t_s \geq \frac{1.3(t_{e1}+t_{e2})F}{A_{re}\sigma_{st}} \geq 2.0\text{ mm} \tag{4}$$

The tensile stresses determined using the minimum thicknesses from Eqs. (3). (4) at 90 MPa from BE1/76 and 58.3 MPa from BS5400 are far higher than the stresses from Eq. (2) and the FEM analysis.

5. Summary and conclusions

A three-dimensional finite element analysis was carried out to investigate the behaviour of elastomeric bearings under combinations of axial compression, shear and rotation. The analytical results under axial load, axial and shear load, and axial and rotation load were found to be in good agreement with the experimental results from bearing tests carried out under similar loads. This agreement between the analytical and experimental results enables the analytical results to be used to make predictions about the state of stress within the bearing - something

that could not be investigated experimentally. The total shear strain in the rubber layers determined by the numerical finite element analysis were compared with the values given by the various bearing design methods.

The bulging deformation at the edges of the bearing was found to introduce high tensile and shear strains at the interface between an inner rubber layer and a steel shim. The tensile strain grew more rapidly than the shear strain as the loading magnitude increased under all of the loadings studied and the bulging effect became extremely marked as the loading level increased.

The cover rubber of the bearing resists the bulging deformation of the rubber layers and therefore must suffer even larger shear strains than the inner rubber layers. From the numerical study, the cover rubber showed a more than 50% larger shear strain than the inner rubber layers at a bearing shear strain of 106%.

From both the experimental results (Mori, *et al.* in press 1997a,b) and the results reported herein, it appears that the steel shims within the bearing would reach their yield stress at somewhere between 106% and 150% bearing shear strains. It is possible that the steel shims could yield during an earthquake should it be large enough to cause bearing shear strains of this magnitude or larger. If the bearings undergo many cycles of shearing with relatively large amplitudes, the steel shims could fail in fatigue. However, bearing performance in terms of the force-displacement response may not be greatly affected by damage of the steel shims as long as the steel shims can properly transfer the shear stress to the rubber layers.

The analytical results for the bearing under tensile load indicated that the lateral tensile strain in the rubber grew very rapidly even if the change in the tensile force was small and this could lead to rupture of the rubber. The rapid growth of the lateral tensile strain in tension is much more marked than in the other loading states.

It was difficult to adequately assess the various bearing design methods since they are partially based on empirical relationships in order to be convenient for design. The equation used in the bearing design codes to evaluate the maximum shear strain in the rubber due to compression was reasonably accurate when compared to the analytical results providing the coefficient for the bearing shape was taken as 6.0 in both the BE1/76 and AASHTO methods and the loading magnitude did not greatly exceed the design load level. However, the superposition technique used in the design methods for obtaining the maximum total shear strain under the various combinations of loading appeared to be very conservative.

Numerical difficulties associated with the degree of mesh refinement of the finite element model meant that the analyses could not be carried out to reach the ultimate bearing deformation.

References

AASHTO, (1990), "Guide specification for seismic isolation design of highway bridges", Washington, DC, USA.

ABAQUS, (1992), Hibbit, Karlsson and Sorensen Inc, USA.

Atkin, R.J. and Fox, N. (1980), "An introduction to the theory of elasticity", Longman.

British Standards Institution, (1983), "BS5400: Steel, concrete and composite bridges, Parts 9A and 9B".

Ghent, A.E. and Meinecke, E.A. (1970), "Compression, bending and shear of bonded rubber blocks", *Polymer Engineering and Science,* **10**(1), 48-53.

Highways Directorate, Department of Environment (1976), "Design recommendations for elastomeric bearings", *Technical Memorandum* BE1/76, Great Britain.
Ministry of Construction, (1992), *Guidelines for Design of Base-Isolated Highway Bridges*, Tokyo, Japan, (in Japanese).
Mori, A. (1993), "Investigation of the behaviour of seismic isolation systems for bridges", Ph.D thesis, University of Canterbury, Christchurch, New Zealand.
Mori, A., Carr, A.J., Cooke, N. and Moss, P.J. (1996), "The compression behaviour of bearings used for seismic isolation", *Engineering Structures*, **18**(5), 351-362.
Mori, A., Carr, A.J., Cooke, N. and Moss, P.J. (in press 1997a), "The behaviour of bearings used for seismic isolation under shear and axial load", *Earthquake Spectra*.
Mori, A., Carr, A.J., Cooke, N. and Moss, P.J. (in press 1997b), "The behaviour of bearings used for seismic isolation under rotation and axial load", *Earthquake Spectra*.
Stanton, J.F. and Roeder, C.W. (1982), "Elastomeric bearings, design, construction and materials", *NCHRP Report* 248, Washington, D.C., USA.
Treloar, L.R.G. (1958), *The Physics of Rubber Elasticity*, 2nd Ed., Oxford University Press.

Appendix A

a) Maximum shear strain due to compression

In design, the maximum shear strain, γ_c, due to bulging in compression is calculated assuming constant volume to give the maximum value at the bearing edge in plane dimensions as

$$\gamma_c = C_c S \varepsilon_c \quad \text{for BE1/76, Japanese Manual \& AASHTO} \tag{A1}$$

$$\text{where } \varepsilon_c = \frac{F}{A_{re} E_c} \tag{A2}$$

$$\text{or } \gamma_c = \frac{1.5F}{G_a A_{re} S} \quad \text{for BS5400} \tag{A3}$$

Here; C_c is the coefficient for bearing shape, S is the shape factor of an elastomer layer in the bearing, ε_c is the bearing compressive strain, E_c is the compression modulus of the rubber calculated using one of Eqs. (A5)-(A7) (see also Table A1).

C_c is taken as 6.0 in BE1/76, AASHTO and Japanese manual, though in the latter, a value of 8.5 is to be used for rectangular bearings.

The shape factor S is calculated as

$$S = \frac{L_e W_e}{2t_e(L_e + W_e)} \quad \text{for a rectangular bearing} \tag{A4}$$

where L_e and W_e are the effective length and effective width and are equal to the length and width respectively of the inner steel shims, while t_e is the thickness of a rubber layer.

The reduced effective cross-sectional area, A_{re} is equal to $(L_e \times W_e)$ for compression but will differ under shear as W_e will need to be reduced by the amount of lateral displacement produced by the shearing action (Mori, *et al.* in press 1997a).

Values for the compression modulus of elasticity of the rubber, E_c, are:

(i) BE1/76 (1976)

$$E_c = E(1 \times 2kS^2) \tag{A5}$$

where E_c is the compression modulus of an elastomer, E is the Young's modulus of an elastomer, k is the constant dependent on the hardness of an elastomer and S is the shape factor of an elastomer layer.

(ii) BS5400 (1983)

$$E_c = 5G_a S^2 \tag{A6}$$

where G_a is the apparent shear modulus of an elastomer.

(iii) Japanese design manual for highway bridges (Ministry of Construction 1992)

$$E_c = (3.0 + 6.580S^2)G_a \text{ for rectangular bearings} \tag{A7}$$

Table A1 Coefficients and equations in Eqs. A1 and A2 for each design method

Term	BE1/76	Japanese manual	AASHTO guide specification
C_c	6.0	8.5 for rectangular bearings 6.0 for circular bearings	6.0
E_c	$E(1+2kS^2)$	$G_a(3+6.58S^2)$ for rectangular bearings $G_a(3+4.935S^2)$ for circular bearings	$E(1+2kS^2)$

b) Maximum shear strain due to shear

The maximum shear strain, γ_s, due to shear is calculated from

$$\gamma_s = \frac{\delta_s}{\sum t_e} \tag{A8}$$

where γ_s is the lateral relative displacement of the bearing and t_e is the thickness of an elastomer layer of the bearing.

c) Maximum shear strain due to rotation

The maximum shear strain, γ_r, due to rotation is calculated from

$$\gamma_r = \frac{W_e^2 \theta}{2t_e \sum t_e} \tag{A9}$$

for BS5400 (1983) and AASHTO (1990) specifications.

From the Japanese manual (1992),

$$\gamma_r = \frac{2(1+\beta)^2}{\beta^2} S^2 \alpha_e, \quad \beta = \frac{L_e}{W_e} \text{ for rectangular bearings} \tag{A10}$$

where W_e is the effective width of the bearing, θ is the angle of rotation of the bearing, L_e is the effective length of the bearing and α_e is the angle of rotation for an elastomer layer of the bearing.